• Review •

Formation and Variation of the Atmospheric Heat Source over the Tibetan Plateau and Its Climate Effects

Guoxiong WU[1,2], Bian HE[*1,2], Anmin DUAN[1,2], Yimin LIU [1,2], and Wei YU[1,3]

[1]*State Key Laboratory of Numerical Modeling for Atmospheric Sciences and Geophysical Fluid Dynamics,*
Institute of Atmospheric Physics, Chinese Academy of Sciences, Beijing 100029, *China*
[2]*University of Chinese Academy of Sciences, Beijing* 100029, *China*
[3]*School of Atmospheric Sciences, Nanjing University, Nanjing* 210093, *China*

ABSTRACT

To cherish the memory of the late Professor Duzheng YE on what would have been his 100th birthday, and to celebrate his great accomplishment in opening a new era of Tibetan Plateau (TP) meteorology, this review paper provides an assessment of the atmospheric heat source (AHS) over the TP from different data resources, including observations from local meteorological stations, satellite remote sensing data, and various reanalysis datasets. The uncertainty and applicability of these heat source data are evaluated. Analysis regarding the formation of the AHS over the TP demonstrates that it is not only the cause of the atmospheric circulation, but is also a result of that circulation. Based on numerical experiments, the review further demonstrates that land–sea thermal contrast is only one part of the monsoon story. The thermal forcing of the Tibetan–Iranian Plateau plays a significant role in generating the Asian summer monsoon (ASM), i.e., in addition to pumping water vapor from sea to land and from the lower to the upper troposphere, it also generates a subtropical monsoon–type meridional circulation subject to the angular momentum conservation, providing an ascending-air large-scale background for the development of the ASM.

Key words: atmospheric heat source, Tibetan Plateau, climate effect, uncertainty

1. Introduction

For a long time, the Tibetan Plateau (TP) has been visualized as an elevated heat source in summer, based originally on the reports of explorers that cumulonimbus and severe convective weather occur frequently in this season. A field observation during the Italian Expedition in 1914 at Depsang (35.3°N, 78.0°E) (Alessandri and VenturiGinori, 1931; also refer to Flohn, 1957) confirmed this visualization: "... In summer near noon the average atmospheric lapse rate may be dry-adiabatic in the boundary layer, near moist-adiabatic above the condensation level, and slightly supper-adiabatic in the lowest 100–200 m". These observations were summarized in a paper by Flohn (1957), in which the author, based on observational data, also reported the existence of "... a thermal anticyclonic cell in the mid troposphere above the Highland". The year of 1957 was destined to be memorable in the study of the climate impacts of the TP. Prior studies had treated the TP mainly as a dynamical obstacle. However, that year, it was YE and his colleagues (Yeh et al., 1957) who first

recognized and formulated mathematically the heat source of the TP and its weather and climate effects. In the same year, besides these pioneering studies, many scholars investigated the circulation, heat sources, and atmospheric thermal balance in the area surrounding the TP, revealing their impacts on the distribution of temperature and circulation over Asia (Chu, 1957a, 1957b, 1957c; Yang and Lo, 1957). Indeed, a new era of TP meteorology had commenced.

Local change in atmospheric potential temperature (PT) is determined by its horizontal advection, vertical convection or adiabatic process, and the atmospheric heat source (AHS). Based on synoptic diagnosis of the late spring period from 12 May to 12 June, and of the mature monsoon period from 7–16 July in 2008, Seto et al. (2013) showed that horizontal PT advection in the upper troposphere above 250 hPa is important for local PT change, and vertical moist convection in association with latent heat (LH) is essential in the middle troposphere from 450–250 hPa. Using observations from a field experiment at the observation site BJ(31.4°N, 91.9°E) over the eastern TP in the pre-monsoon season of 2004, Taniguchi and Koike (2007) identified a significant diurnal PT increase near the tropopause in the afternoon, and showed that it coincided with active cumulus convection. On the other hand,

---

* Corresponding authors: Bian HE
  Email: heb@lasg.iap.ac.cn

from May to August in the upper troposphere, there is a warm area located to the southwest of the TP. Data diagnosis, numerical simulation and theoretical study by Tamura et al. (2010), Taniguchi et al. (2012), and Wu et al. (2015b) all revealed that this upper-tropospheric warm center is formed due to significant adiabatic air descent accompanied by remarkable flow convergence aloft. This convergence flow is linked with the upper-tropospheric divergent flow induced by strong and heavy convection in the tropical Indian Ocean from the south, and by those in the East Asian monsoon area from the east and southeast.

The AHS affecting the local PT change includes radiative heating/cooling from the atmosphere and the Earth's surface, LH release due to condensation, and diffusive sensible heat (SH). For decades, many studies have been devoted to understanding the AHS over the TP and the surrounding area, and its weather and climate impacts (Luo and Yanai, 1984; Chen et al., 1985, 2003; Yanai et al., 1992; He et al., 2011). Accordingly, several consensuses have been reached, as summarized below:

• Over the TP, the AHS is negative in winter and positive in summer;

• Before the onset of the Asian summer monsoon (ASM) and over the TP, surface sensible heating prevails over the LH release in the free atmosphere, and the SH flux prevails over the LH flux at the ground surface;

• During ASM months, LH release due to condensation dominates over the southern and eastern TP, whereas SH dominates over the western TP;

• The LH release of the ASM in the region south of the TP and over the northern Bay of Bengal (BOB) is much stronger compared to the SH over the TP (Chen and Li, 1981, 1982). However, as discussed by Kuo and Qian (1982), this heat source is induced by the TP forcing;

• The variation in the AHS over the TP takes place on a variety of time scales, either induced by the TP heating itself (e.g., Zhang et al., 1991; Liu et al., 2007) or due to interaction between the thermal status of the TP and the atmospheric circulation (Duan and Wu, 2008, 2009).

• Monsoon is usually considered as a consequence of the atmospheric response to the seasonal change in land–sea thermal contrast (Li and Yanai, 1996; Webster et al., 1998; Liang et al., 2005). The AHS of the TP and its variability can also strongly affect the ASM, as well as the weather and climate in Asia and even over the Northern Hemisphere (Zhao and Chen, 2001; Wu et al., 2015a).

Because of the sparseness of observational data, the low accuracy of remote sensing data, and the model-dependence of reanalysis data, the above consensuses remain qualitative. Besides, how the SH over the TP is formed and how it varies in accordance with other climate systems has yet to be explored in sufficient depth. In this review, a brief introduction of the AHS over the TP is presented in section 2. Specifically, the uncertainty and applicability of different kinds of data over the TP are evaluated, and the general nature of the AHS over the TP, including its elevation-dependence, is demonstrated. In section 3, the formation and variation of the AHS over the TP in different seasons is discussed. The variation of the surface sensible heating over the TP during the ASM onset in 1989 and its attribution are also reviewed. The mechanisms underlying the impacts of the AHS on the ASM and climate are presented briefly in section 4, followed by concluding remarks in section 5.

2. AHS over the TP

2.1. *Data quality: uncertainty and applicability*

Recently, Duan et al. (2014) provided a comprehensive report on the uncertainty in quantitative estimation of the AHS over the TP, and concluded that the uncertainty comes not only from the sparseness of meteorological observations, but also from the different elevations of the observing stations. Figure 1a shows that most of the 73 meteorological stations over the TP are located its center and east (east of 85°E), with only two stations in its west. Based on a 5-km high-resolution (2160×1081) orography dataset retrieved from the U.S. Navy Fleet Numerical Oceanography Center, they further demonstrated that the number of grids with elevations higher than 5 km MSL in the TP domain (25°–40°N, 75°–105°E) accounts for 31% of the total grid number in the domain, and the number of grids higher than 4 km accounts for 64% of the total. However, none of the meteorological stations is located above 5 km, and only 17 stations are located above 4 km. Consequently, a large area is not included in the dataset. Besides, no direct observations of surface heat flux and vertical heating profiles at most stations also contributes to the problem.

Reconstructed data on surface fluxes, atmospheric variables, and radiation, based on satellite remote sensing, are frequently used for presenting the AHS (e.g., Duan and Wu, 2008; Yang et al., 2011a, 2011b; Ma et al., 2014a, 2014b). However, these data suffer from problems relating to accuracy and temporal and spatial coverage, and usually need to be calibrated. Reanalysis data can provide both temporally and spatially continuous data series and are widely employed in presenting the thermal status of the TP. However, various model errors can result in a model-dependent climate that may deviate from reality and lead to serious biases. Zhu et al. (2012) analyzed the spatial distribution of summertime (June– August) averaged surface SH flux from eight data sources. These datasets included five reanalysis datasets (NCEP-1, NCEP-2, CFSR, JRA-25, and ERA-40), two land surface model outputs [G2_Noah, GLDAS; and version 2 SiB (SiB2) output by Yang et al. (2009, 2011a; YSiB2)], and estimated SH based on China Meteorological Administration station observations (ObCh). The results, shown in Fig. 2, demonstrated that the distribution pattern varied from one set to another, with the assimilated one (YSiB2, Fig. 2g) based on the land surface model (SiB2) closest to the "observed" estimates (Fig. 2h).

2.2. *Applicability and variability*

Zhu et al. (2012) compared eight datasets of summer
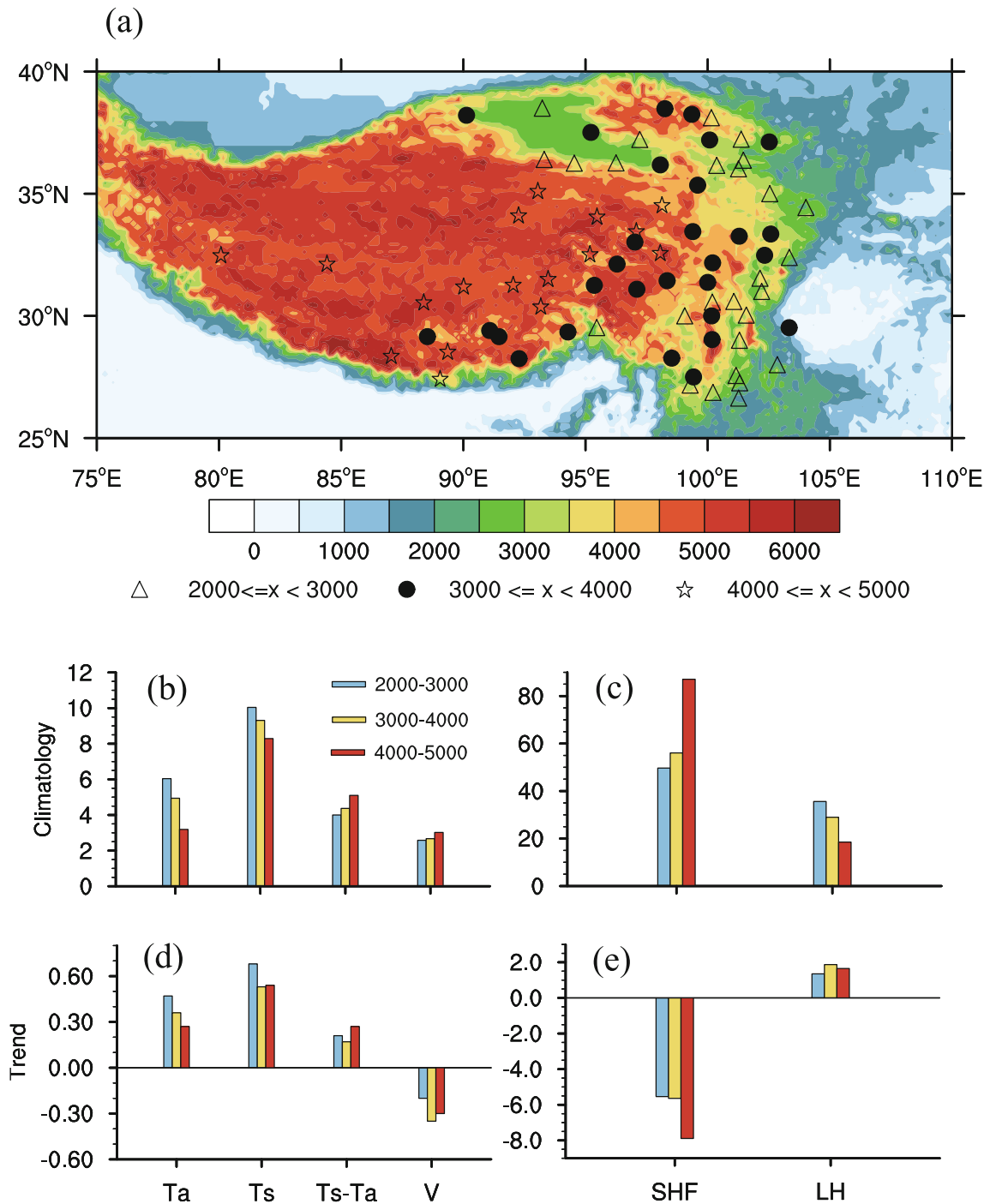
Fig. 1. (a) Terrain height (units: m) over and around the TP and the locations of 73 meteorological stations across the TP. Open triangle, solid circles, and stars denote the stations with elevations at 2–3 km, 3–4 km, and 4–5 km, respectively. Elevation-dependence of the (b, c) spring mean and (d, e) linear trend of the T_a, T_s, $T_s - T_a$ [units: °C and °C (10 yr)$^{-1}$], V [units: m s^{-1} and m s^{-1} (10 yr)$^{-1}$], and local surface SH flux (SHF) and LH released to the atmosphere due to condensation [units: W m^{-2} and W m^{-2} (10 yr)$^{-1}$], during 1984–2007, and averaged from 71 stations over the central and eastern TP. The trends are statistically significant at the 95% confidence level. The blue-, yellow-, and red-colored bars in (b–e) are for the areas with terrain height of 2–3 km, 3–4 km, and 4–5 km, respectively.

(June–August) mean surface SH flux averaged over the TP in terms of their climatology, interannual variability and linear trend during 1980–2006. They reported serious differences in the distribution patterns of surface SH flux, and concluded these differences were due to the different climate biases among the various models. However, when studying the intrinsic variability, they found that a dataset averaged over the TP can successfully present the variability because, by removing the models' mean climate, the model bias can to a large extent be eliminated. Figure 3 shows the interannual
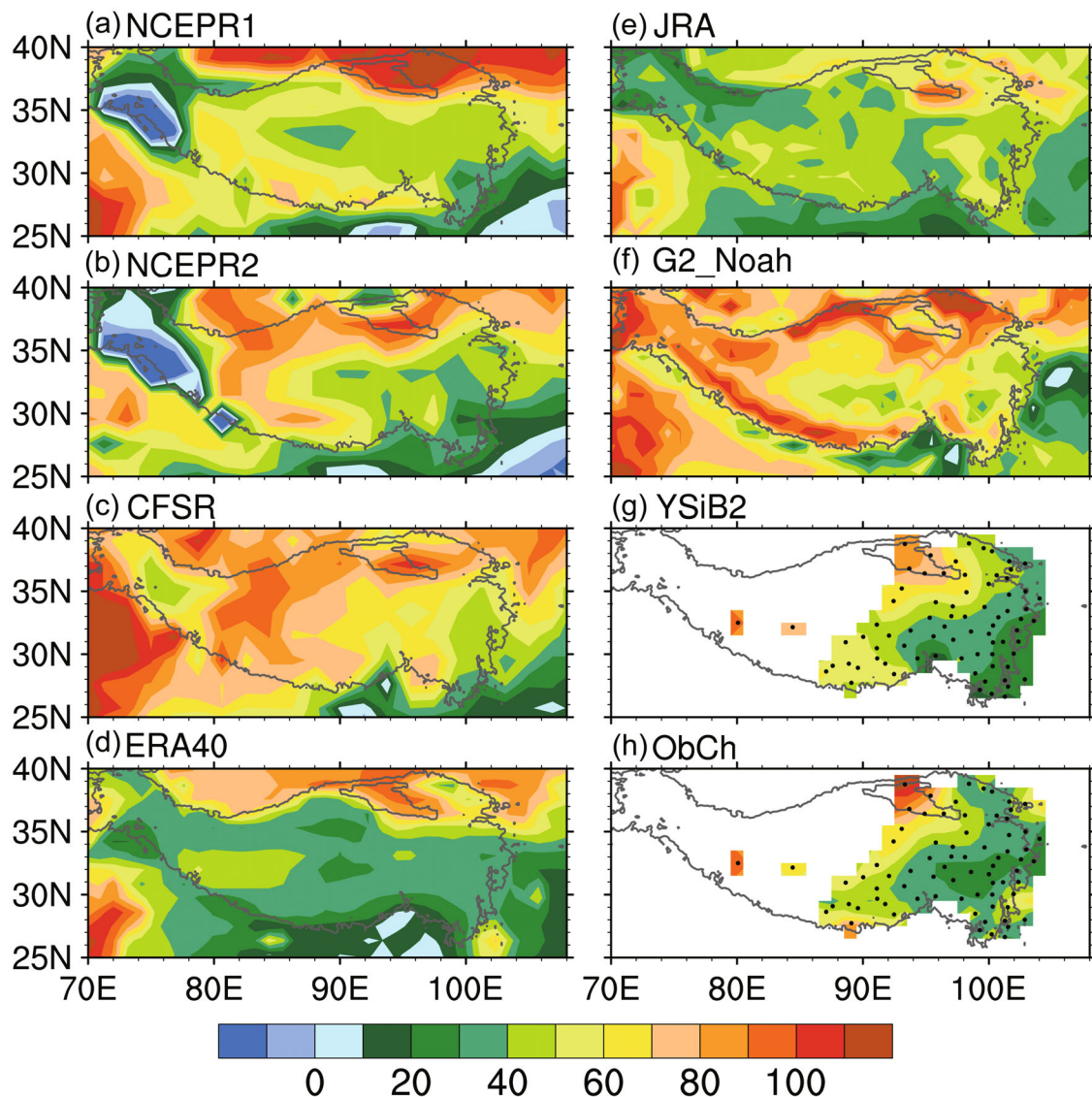
Fig. 2. Spatial distribution of the climatology of summer (June–August) mean SH flux on the TP from eight sources (units: W m^{-2}): (a) NCEP-1; (b) NCEP-2; (c) CFSR; (d) ERA-40; (e) JRA-25; (f) G2_Noah; (g) YSiB2; (h) ObCh. The black curve stands for 3000 m height and dark circles for stations; see text for details. [Reprinted from Zhu et al. (2012)].

variation and linear trends of the summertime surface SH flux (Fig. 3a), ground-air temperature difference (Fig. 3b), and wind speed at 10 m above the surface (Fig. 3c), averaged over the TP. The results demonstrate that good agreement exists among different datasets in terms of the interannual variation and climate trend. This is significant because it implies it is possible to use the area-mean AHS averaged over the TP in different datasets as an index to study the variability of the AHS over the TP and its climate impacts. This is because the model-induced systematic bias of the dataset concerned can be substantially reduced when temporal variation is studied.

2.3. *AHS over the TP and its elevation-dependence*

The above conclusion has been supported by a series of studies. Figure 4 presents the July-mean vertical profiles of various kinds of heating averaged over the western TP (29°–

38°N, 78°–90°E) and eastern TP (27°–40°N, 90°–105°E), based on NCEP reanalysis data (Wu et al., 2009). The profiles share similar features: in summer, the AHS is positive below $\sigma = 0.8$ (terrain following coordinate) over the west and $\sigma = 0.7$ over the east, and almost vanishes aloft. The atmospheric cooling comes from longwave radiation, with a maximum cooling of 4 K d^{-1} over the west and 3 K d^{-1} over the east at $\sigma = 0.85$, indicating the existence of an inversion layer below $\sigma = 0.85$. All other processes, including shortwave absorption, vertical diffusive heating, large-scale latent heating and convective heating, contribute to the positive AHS over the TP. Whilst large-scale latent heating with a warm maximum of about 4 K d^{-1} dominates in the lower troposphere, convective heating with a warm maximum of about 2 K d^{-1} prevails in the upper troposphere. The most remarkable feature is the existence of a huge diffusive sensible heating of
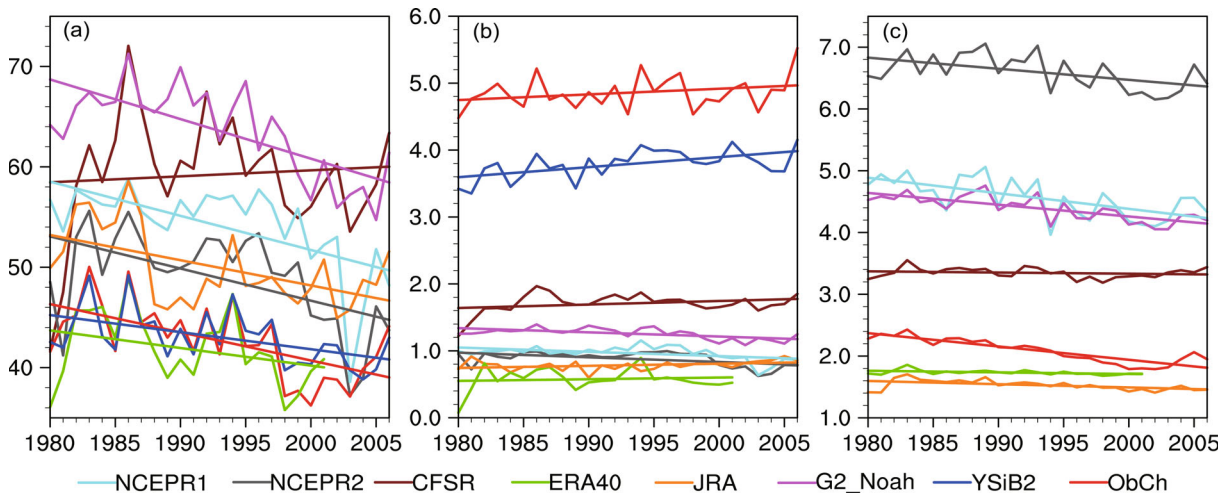
Fig. 3. Interannual variation and linear trends of the summer (June–August) mean (a) surface SH flux (units: W m^{-2}), (b) ground-air temperature difference (units: K), and (c) wind speed at 10 m (units: m s^{-1}), averaged over 76 stations on the TP. [Reprinted from Zhu et al. (2012)].
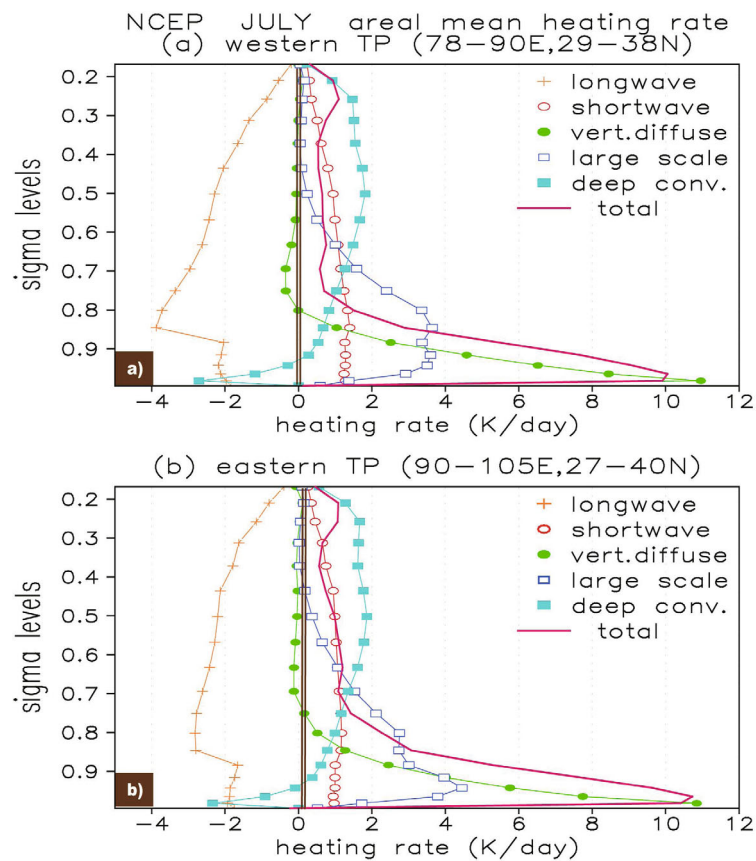
Fig. 4. The 1980–97 July-mean vertical heating profiles over (a) the western TP area (29°–38°N, 78°–90°E) and (b) the eastern TP area (27°–40°N, 90°–105°E), based on NCEP–NCAR reanalysis data (units: K d^{-1}). Lines with "plus" signs, open circles, filled circles, open squares, and filled squares represent longwave radiative cooling, shortwave radiative heating, vertical diffusive heating, large-scale condensation heating, and convective condensation heating, respectively. Red solid lines indicate total heating. [Reprinted from Wu et al. (2009)].

11 K d^{-1} located at the surface. As will be discussed, such a strong surface sensible heating imposes great influence on the regional and even global climate. The results shown in Fig. 4 demonstrate the main similarities in the vertical distributions of different components of the AHS between the eastern and western parts of the TP, whilst at the same time revealing the existence of small differences between the two parts in their finer detail. It is worth noting that, in the process of reanalysis, surface observations are included for assimilation. Therefore, the accuracy of reanalysis data for the eastern part of the TP is expected to be better than for the western part, because of the greater density of surface observations.

The AHS over the TP is elevation-dependent. As shown by Duan et al. (2014), whilst the surface air temperature (T_a) and surface ground temperature (T_s) decrease with increasing elevation of the TP, the surface wind increases with height (Fig. 1b). Accordingly, the surface SH flux increases with height (Fig. 1c), and reaches almost 100 W m^{-2} at the 4–5-km layer. Because the surface sensible heating depends on the surface wind speed and the temperature difference between the underlying ground surface and surface air, i.e., $T_s - T_a$, and because with increasing height the T_a decreases faster than the T_s, as shown in Fig. 1b, the increasing surface SH flux with increasing elevation is not only due to the increas-

ing wind speed, but also to the increasing land–air temperature difference ($T_s - T_a$). In general this is true because, under the convective–radiative-equilibrium constraint (Molnar and Emanuel, 1999), the lapse rate of T_s is estimated to about 3 K km^{-1}, which is smaller than the normal atmospheric lapse rate of 6 K km^{-1}. On the other hand, the LH released to the atmosphere due to condensation in cloud decreases with increasing height, since less water vapor is contained within a more elevated atmospheric column, and since the convergence of water vapor flux is much stronger in low layers than in high layers of the atmosphere. The linear trends also change with different TP elevation (Figs. 1d and e). Both the T_a and T_s warming is stronger at lower than higher elevations (Fig. 1d), while the surface wind speed shows a weakening trend in all layers. Accordingly, the surface sensible heating is weakened in all layers, with the greatest weakening being about 8 W m^{-2} (10 yr)$^{-1}$ and occurring in the highest layer of 4–5 km (Fig. 1e); whereas, the LH over the TP presents a weak increase of less than 2 W m^{-2} (10 yr)$^{-1}$ in all layers.

2.4. AHS over the TP in different data resources

Duan et al. (2014) also compared different reanalyses in terms of their spring means and linear trends of the AHS and its components over the TP, as shown in Fig. 5. Good
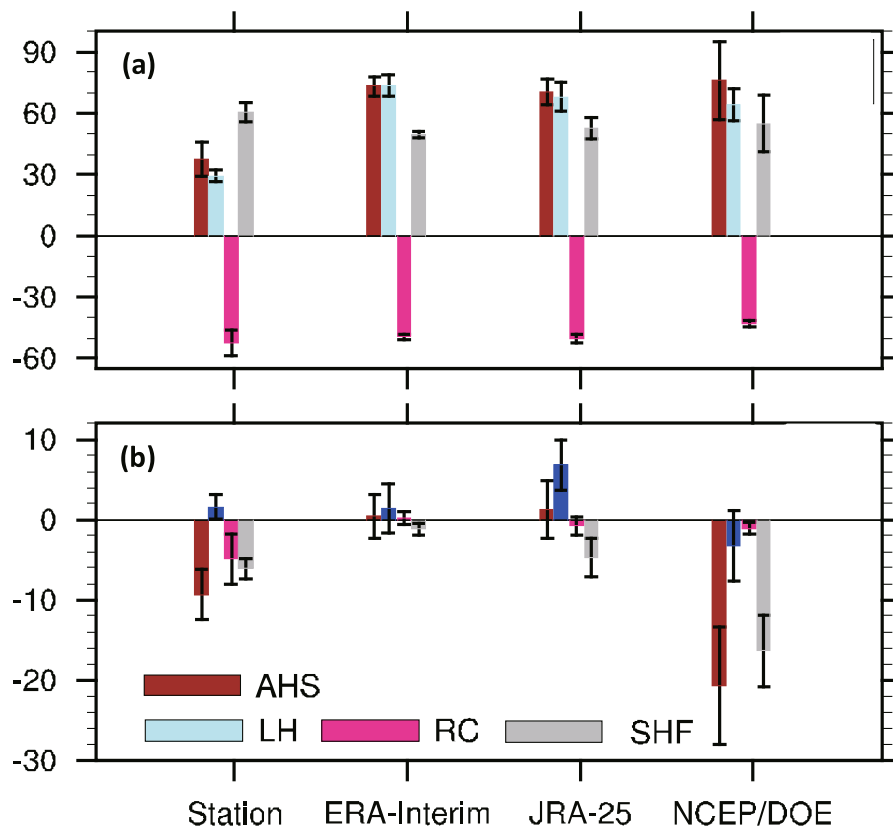
Fig. 5. The (a) spring mean and (b) linear trend of the AHS, LH, RC, and SHF over the central and eastern TP during 1984–2007, determined on the basis of observational data and three reanalysis datasets. Units for the climate mean and trend are W m^{-2} and W m^{-2} (10 yr)$^{-1}$, respectively. Bars indicate uncertainty at the 95% confidence level, based on standard deviation. All results in the reanalysis data have been interpolated onto the locations of 71 stations and ISCCP radiation flux data to estimate RC at the stations. [Reprinted from Duan et al. (2014)].

agreement exists in the climate means among three reanalysis datasets (Fig. 5a): in spring, the LH is stronger than the surface sensible heating, and the total AHS over the TP is more than 70 W m^{-2}. Compared to station data, these reanalysis data share the same bias: the condensation heating and the total AHS are overly strong, while the surface sensible heating is excessively weak. On the other hand, Fig. 5b demonstrates a decreasing trend in surface SH flux in both observation and reanalysis, which is in good agreement with the results obtained by Zhu et al. (2012), as shown in Fig. 3, wherein the decreasing trend of the surface sensible heating is shown to be mainly due to the weakened surface wind during the study period. However, significant discrepancies among different datasets exist with respect to the trend estimation of the LH, the radiative heating (RC), and the total AHS.

3. Formation and variation of the AHS over the TP

Most previous studies assumed the TP as a heat source and then investigated its impacts on weather and climate. However, the climate system is a nonlinear, open, and dissipative system involving multi-sphere interactions. The variation of weather and climate in a region is usually caused simultaneously by different factors. For instance, the per-

sistent occurrence of the "south-flood–north-drought" pattern over East China from the 1980s to the beginning of the 21st century is attributed to the interdecadal weakening of the TP thermal forcing (Duan and Wu, 2008; Liu et al., 2012; Wu et al., 2012a), but is also well interpreted by the interdecadal change of the western Pacific subtropical high (Zhou et al., 2009). This implies the existence of coordinative impacts on the East Asian summer monsoon from the two systems. In other words, the formation of the AHS over the TP should be closely related with the atmospheric circulation in the coupled climate system.

3.1. *Wintertime AHS over the TP*

In winter, strong westerly flow impinges upon the TP directly, and mechanical forcing should prevail over its thermal impact (Held, 1983). However, condensation heating still exists, particularly over its western and southern rims. By applying EOF analysis to ERA-40 data, Yu et al. (2011a, 2011b) identified the first EOF of the AHS over the TP as the condensation heating over its southwestern slope (Fig. 6a), and its regressed 500-hPa circulation presents a wave train emanating from the North Atlantic in association with the North Atlantic Oscillation (Fig. 6b). A cyclonic circulation center of this wave train is located to the west of the TP, with strong west-southwesterly flow located to the southwest
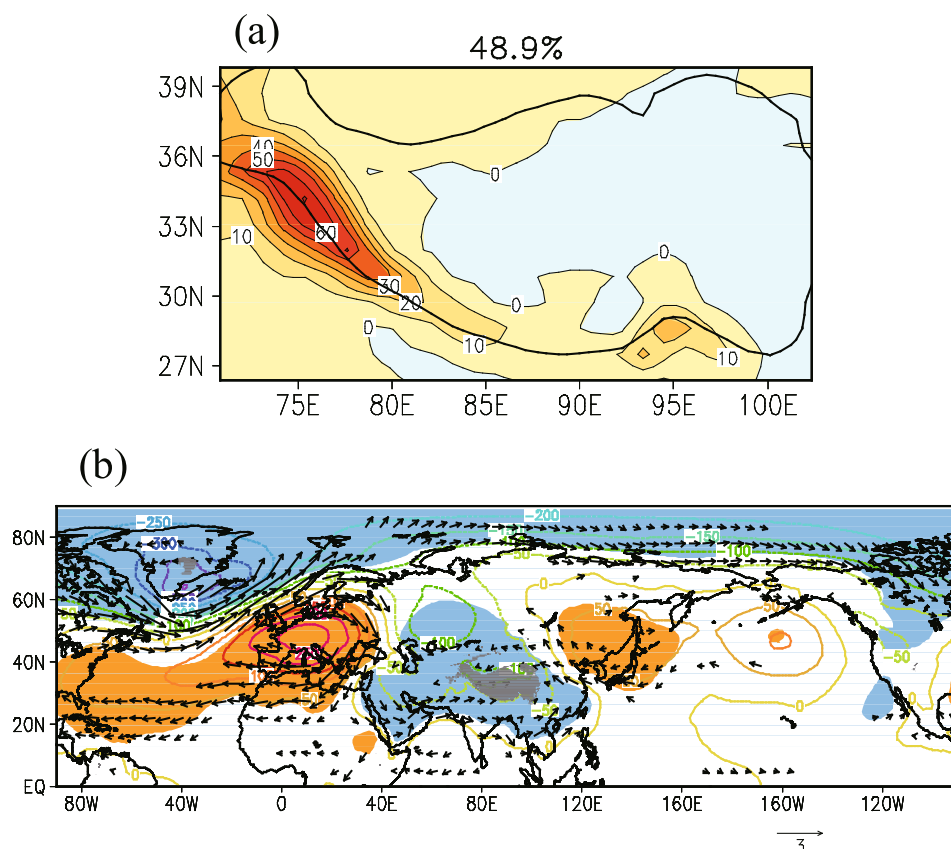
Fig. 6. Distributions of (a) the first interannual variation mode of the column-integrated diabatic heating in January over the TP, and (b) the regressed 500-hPa wind and geopotential height exceeding the 95% confidence level (shading; orange and blue coloring indicates positive and negative, respectively), based on ERA-40. [Reprinted from Yu et al. (2011b)].

of the TP, which generates upslope ascending flow over the southwestern TP and thereby produces a heat source in that region. Thus, the AHS over the TP in winter is formed due to a specific atmospheric circulation.

3.2. *Intra-seasonal oscillation of the circulation and the AHS over the TP*

There is a spectacular occurrence of persistent rainfall over southern China in early spring from March to May (hereafter, PRES) (Tian and Yasunari, 1998). Wan and Wu (2007) demonstrated that the occurrence of PRES is mainly due to a certain type of TP forcing in early spring in which cold northerly advection and warm and moist southerly advection meet over South China, resulting in persistent rainfall in that region. By applying EOF analysis to the daily rainfall anomaly time series in southern China for the period March–May from 1980 to 2008, Pan et al. (2013) found that PRES possesses a pronounced 10–20-day intraseasonal oscillation (ISO). During the dry phase, PRES is inactive and less than normal rainfall occurs over South China, and vice versa. They also found that, during the dry phase, the TP is a heat sink, which induces surface divergent flow from the central TP extending eastwards to South China, leading to descending air and reduced precipitation locally (Fig. 7a). During the wet phase, the TP is a heat source, which induces surface convergent flow from the central TP extending eastwards to South China, leading to in-situ ascending air and intensified local precipitation (Fig. 7d). The results demonstrate that TP surface sensible heating/cooling plays a significant role in controlling the nature of PRES. Further diagnosis of their results shows that, during the dry/wet phase at 500 hPa, a warm anticyclone/cold cyclone occupies the TP region (Figs. 7b and e). From the longitude–height cross section averaged over 30°–40°N, as shown in Figs. 7c and f, a prominent baroclinic Rossby wave pattern can be identified, i.e., the temperature field lags the geopotential height field and tilts westwards with increasing height. During the dry phase (Fig. 7c), the western TP is in front of a trough accompanied by ascending air, whereas the area from the central TP to eastern China is behind another trough accompanied by descending air. Conversely, during the wet phase (Fig. 7f), the western TP is in front of a ridge accompanied by descending air, whereas the area from the central TP to eastern China is behind another ridge accompanied by ascending air. During the dry/wet phase, warm/cold advection dominates the TP surface (Figs. 7c and f), resulting in negative/positive temperature differences between the underlying land and the surface air, as well as downward/upward surface SH flux. Therefore, the surface sensible cooling/heating of the TP during the dry/wet PRES phase can be attributed to the ISO behavior of the baroclinic Rossby wave propagation in the atmosphere.

3.3. *ASM onset and the TP AHS*

Wu and Zhang (1998) showed that, in 1989, in association with the three stages of ASM onset, i.e., the sequential monsoon onsets over the BOB, South China Sea (SCS), and India (IND), the mean temperature at 300 hPa over the TP showed three separate abrupt increments, each being preceded with a period of remarkable increase in surface sensible heating over the TP (Fig. 8a). This is because, during the three-stage onset period, there were synoptic-scale temperature perturbations propagating eastwards from Europe to the TP region along the AB route shown in Fig. 8b. Thus, before each abrupt warming over the TP, there had been cold advection (figure not shown; refer to their Figs. 13 and 14). The three cold episodes of advection into the TP region (which occurred before 22 April, 15 May, and early June, respectively; refer to Fig. 8a and their Fig. 5) resulted in a local increase in the land–air temperature difference, leading to the increase in surface sensible heating. The increased SH over the TP could intensify the surface cyclonic circulation surrounding the TP, which in turn could enhance the transport of water vapor from the Indian Ocean to continental South Asia. In addition, the authors demonstrated that, during this period, a northward propagation of the Madden–Julian Oscillation (MJO) circulation system occurred along the route CD from the southern Indian Ocean, as well as a westward propagation of the three tropical cyclones/typhoons from the northwestern Pacific (120°–140°E) along route EF (refer to their Figs. 13 and 14). The northward propagation of the MJO and the westward propagation of the tropical cyclones were both characterized by strong upper-tropospheric divergence and ascending air. When these low-frequency atmospheric oscillations from different directions were phase-locked over the Asian monsoon area, abundant surface water vapor was uplifted by the strong upper-layer divergence, resulting in severe precipitation. The three-stage procedure of ASM onset was thus produced. These results imply that increased surface sensible heating over the TP before onset of the ASM is also due to the influence of the transient atmospheric circulation.

In summer, the interannual variation of the TP AHS is dominated by LH over its central and eastern parts. Jiang et al. (2016) found that, in July–August, the interannual variation of the AHS over the central and eastern TP is significantly affected by convection around the western Maritime Continent. All the results listed above indicate that the AHS over the TP is not only the source of atmospheric circulation, but is also the result of that atmospheric circulation. To understand the impacts of the TP on weather and climate, we need to consider the TP AHS as part of the climate system.

4. Impacts of the AHS over the TP on the ASM and climate

The elevated TP intersects many isentropic surfaces in the lower troposphere. Along its slope, the surface sensible cooling in winter causes the near-surface air to slide downwards and diverge towards its surroundings, whereas the surface sensible heating in summer results in near-surface air converging towards the TP and sliding upwards. Therefore, the functioning of the seasonal change in TP surface sensible heating looks like a giant air pump standing in the central and eastern Eurasian continent, driving the surrounding air
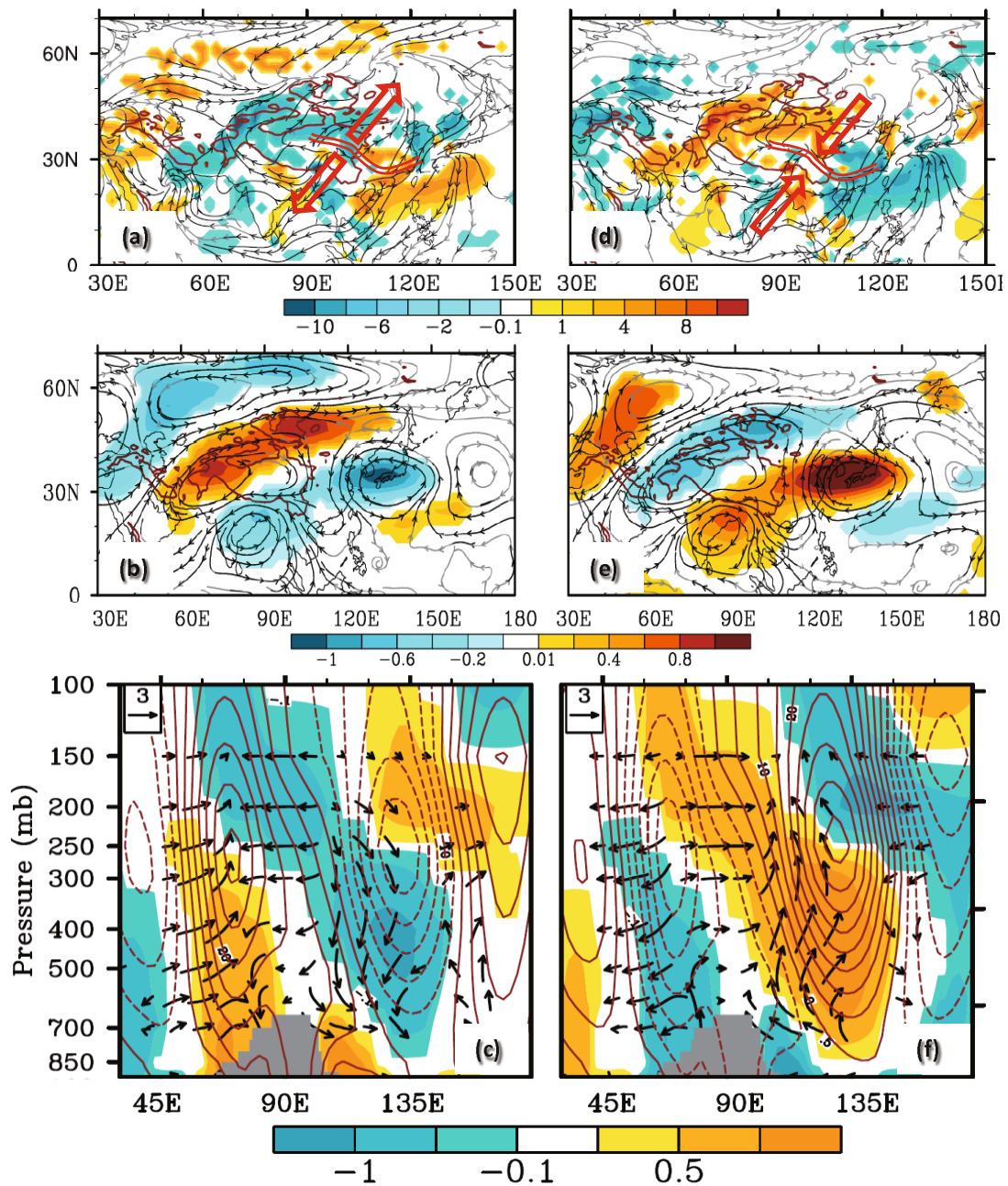
Fig. 7. The 10–20-day filtered meteorological fields for the period March–May from 1980 to 2008: (a, d) 10-m surface streamline and SH flux (shading; units: W m^{-2}); (b, e) 500-hPa streamline and air temperature (shading; units: K); (c, f) the 30°–40°N-averaged pressure–longitude cross sections of air flow (vectors; u in m s^{-1}, and -200ω in Pa s^{-1}), geopotential height (contours; units: gpm), and air temperature (shading; units: K). Panels (a–c) are for the dry phase of PRES over South China, and (d–f) are for the wet phase. The double red curve and blank red arrow in (a) and (d) denote, respectively, the surface divergence/convergence line and flow. Only those results that are statistically significant at the 95% confidence level are shown (shading). The TP with terrain above 1500 m is outlined by the solid red curve in the top and middle panels, and by grey shading in the bottom panels. [Reprinted from Pan et al. (2013)].

masses downwards in winter and upwards in summer, and regulating the seasonal change in the large-scale circulation in Asia. This has been termed the SH- driven air pump, or SHAP in short (Wu et al., 1997, 2007, 2015a). The TP SHAP in summer transports large quantities of water vapor from sea to land and from the lower troposphere to the upper tropo-

sphere to feed the continental ASM (Wu et al., 2012b). This effect was demonstrated well by the different structures of the South Asian summer monsoon (SASM) obtained from a pair of AGCM experiments, as presented in Fig. 9, in which longitudinally averaged (80°–90°E) vertical–meridional cross sections of pressure vertical velocity during summer are
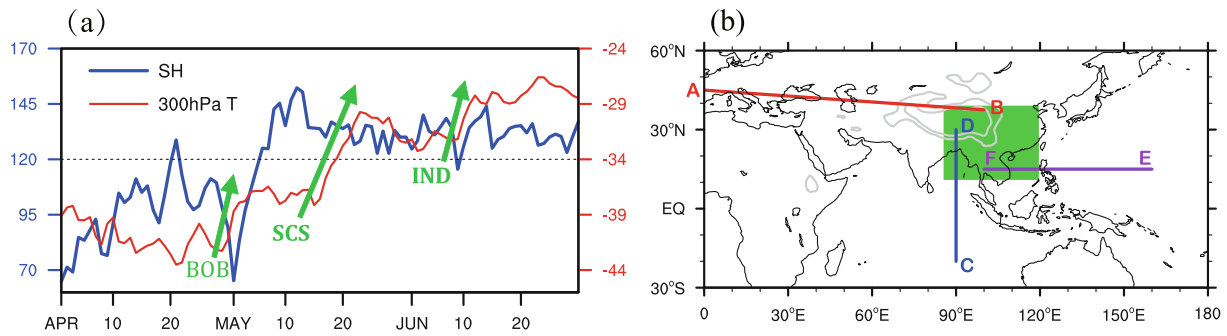
Fig. 8. The (a) evolution of surface SH flux (units: W m^{-2}) and 300-hPa temperature (°C) averaged over the TP and (b) propagation routes of the transient temperature system (AB), the MJO (CD), and tropical cyclones from the northwestern Pacific (EF), during the onset of the ASM (April–June) in 1989. The green arrows in (a) indicate the onset of summer monsoon over the BOB, SCS and IND, respectively. The green shaded region in (b) indicates the locations of the East Asian monsoon area (EAMA) [Reprinted from Wu and Zhang (1998)].
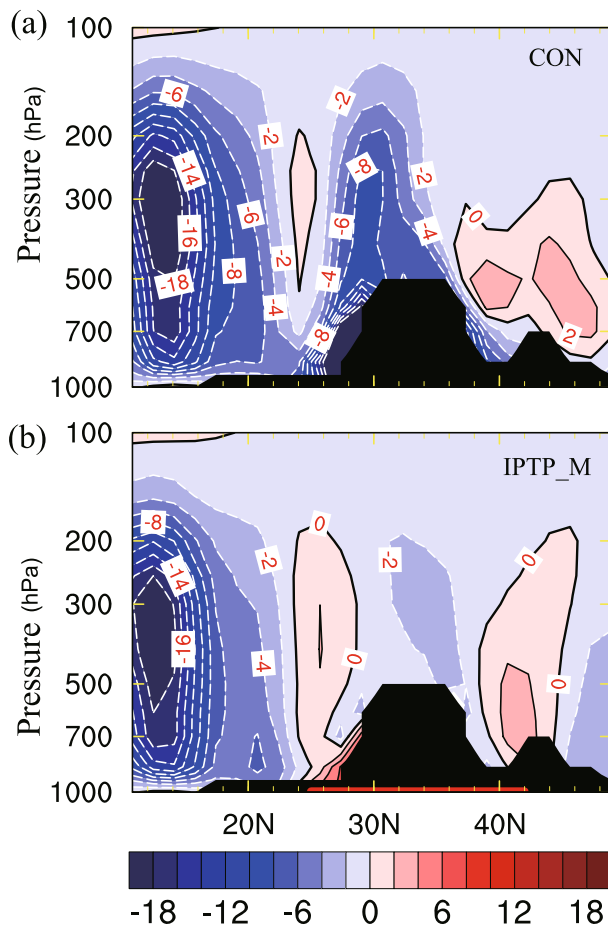
Fig. 9. Structure of the SASM, showing the longitudinally averaged (80°–90°E) vertical–meridional cross sections of pressure vertical velocity (shaded and contour interval: 2×10^{-2} Pa s^{-1}) for experiments (a) CON and (b) IPTP_M, in which the surface sensible heating over the Iranian Plateau and TP was not allowed to heat the atmosphere. The vertical coordinate is in hPa. The black shaded denotes the topography. The thick red line on the bottom of (b) denotes the latitude where surface sensible heating was removed. [Reprinted from Wu et al. (2012b)].

presented. In the control experiment (CON; Fig. 9a), strong ascending motion developed over the northern Indian Ocean and over the southern slope of the TP, representing the southern and northern branches of the SASM, respectively. In the other experiment, IPTP_M (Fig. 9b), which was the same as CON except the surface sensible heating of the Iranian Plateau and TP was not allowed to heat the atmosphere, although strong vertical ascending motion over the northern Indian Ocean associated with the southern branch of the SASM still existed without any significant change in intensity, the ascending motion over the southern slope of the TP, which existed in CON and presented as the northern branch of the SASM, disappeared completely in IPTP_M and was replaced by descending motion. Comparing the results between these two experiments indicates that, without the thermal pumping of the Iranian Plateau and TP, the continental ASM cannot develop. However, how TP forcing contributes to the development of the prevailing ascending motion in the vast ASM area remained unknown.

4.1. *Large-scale ascending motion and regional mean meridional circulation*

The atmospheric vertical motion in summer in the subtropics and in different longitudinal sectors is presented in Fig. 10. Remarkable descending motion prevails over the eastern Pacific region (160°E–90°W), whereas strong ascending motion prevails over the Asian monsoon region (70°–90°E). The distinct difference in vertical motion is closely linked to the distinct difference in meridional circulation in these two regions.

The atmospheric response to an axisymmetric forcing takes two distinct regimes (Schneider and Lindzen, 1977; Schneider, 1977, 1987; Held and Hou, 1980). In the extratropics, the planetary vorticity is large and the Rossby deformation radius is small, where the thermal equilibrium (TE) regime dominates. Whereas, in the tropics, the planetary vorticity is small and the Rossby deformation radius is large; perturbations can develop and even induce meridional circulation, where the angular momentum conservation (AMC)
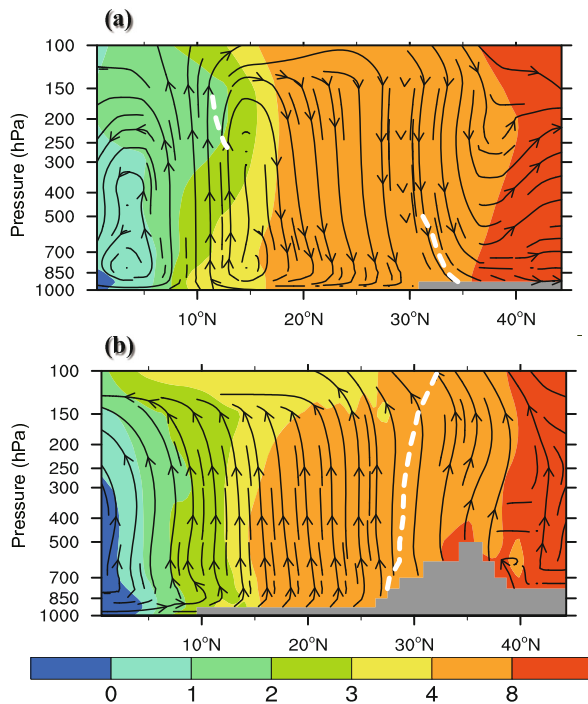
Fig. 10. Cross sections of the July-mean meridional circulation (streamlines), absolute vorticity (units: 10^{-5} s^{-1}; color-shaded), and the zero-zonal wind curve (white dashed line) for the (a) eastern Pacific (160°E–90°W) regional mean and (b) Asian monsoon area (70°–90°E) mean. The vertical coordinate is in hPa. [Reprinted from Wu et al. (2016a)].

regime prevails. Wu et al. (2016a) further demonstrated that the AMC regime can be divided into two types: one is a kind of Hadley meridional circulation (H-AMC, Fig. 10a) with its rising/sinking arm located in the equatorial/subtropical region; and the other is a kind of monsoonal meridional circulation (M-AMC, Fig. 10b) with its rising arm located in the subtropical region. Since the atmospheric vertical motion W is proportional to the vertical change of absolute vorticity advection,

$$W \propto \frac{\partial}{\partial z}[-\boldsymbol{V} \cdot \boldsymbol{\nabla}(f + \zeta)], \qquad (1)$$

where $\boldsymbol{V}$ is horizontal wind, f is the Coriolis parameter, and ζ is relative vorticity, the implication is that an increase/decrease in absolute vorticity advection with increasing height can produce ascending/descending air. Because absolute vorticity advection decreases with height along the H-AMC meridional circulation, and increases with height along the M-AMC meridional circulation, the H-AMC is thus accompanied by descending air and a westerly vertical sheer; whereas, the M-AMC is accompanied by ascending air and an easterly vertical sheer. This implies that the large-scale background of ascending motion in the ASM area must be related to the monsoonal-type meridional circulation, M-AMC. Therefore, in this section, we present the physical basis on how the AHS over the TP plays a significant role in the generation of such a monsoonal-type AMC meridional circulation.

### 4.2. Tropical and subtropical M-AMC meridional circulation

Based on the GCM SAMIL, Wu et al. (2012a) conducted a pair of idealized experiments. One, named TRO, possessed an idealized African–Eurasian continent with the presence of the tropical continents of India and the Indochina Peninsular, by which the southern branch of the SASM was produced along 10°N (Fig. 11a). The other was the same as TRO except an idealized Tibetan–Iranian Plateau (termed TPIR) was added, in which not only the southern branch of the SASM, but also its northern branch to the north of 15°N and the East Asian summer monsoon, were also successfully captured (Fig. 11b). The difference between the results of these two experiments is shown in Fig. 11c, from which it is clearly demonstrated that the land–sea thermal contrast is only one part of the monsoon story, and that the large-scale orography (TP and Iranian Plateau) plays a significant role in the formation of the ASM, particularly the northern branch of the SASM and the East Asian summer monsoon.

The mean meridional circulations $(v, -\omega)$ (v and $-\omega$ denote meridional and vertical velocity, respectively) averaged over the longitudinal domain between 90° and 120°E in these two experiments are shown in Fig. 12. The land–sea thermal contrast in the TRO experiment generates an M-AMC circulation (Fig. 12a); however, this meridional circulation is limited to the tropics, with its rising arm located to the south of 10°N and the descending arm in the southern tropics. In the TPIR experiment, in addition to this tropical meridional circulation, which exists due to the land–sea thermal contrast, a remarkable subtropical M-AMC is generated to the south of 35°N (Fig. 12b). The difference in the results between TPIR and TRO, as shown in Fig. 12c, indicates that the remarkable meridional circulation occurs mainly in the subtropics, just to the south of the TP. It is due to the excitation of this subtropical M-AMC that close coupling between the tropical and subtropical circulations and between the lower and upper tropospheric circulations is established. All these results indicate that it is due to the TP forcing that the subtropical M-AMC is generated.

4.3. SHAP-induced subtropical M-AMC meridional circulation

The atmospheric isentropes are usually horizontally located and intersect with high mountains in the lower troposphere. When an air parcel moves on an isentrope and impinges on the mountain slope, if there is no surface heating on the slope, the air parcel will stay on the same isentropic surface and move horizontally around the mountain. In such a case, there is no ascending air, no cloud formation, and no precipitation. If there is surface sensible heating on the slope, according to SHAP theory, the air parcel will be heated by the surface and pumped upwards from the low PT level to the high PT level. Ascending air is thus induced on the windward side of the mountain, as shown in Figs. 12b and c.

But how can TP thermal forcing generate such a strong
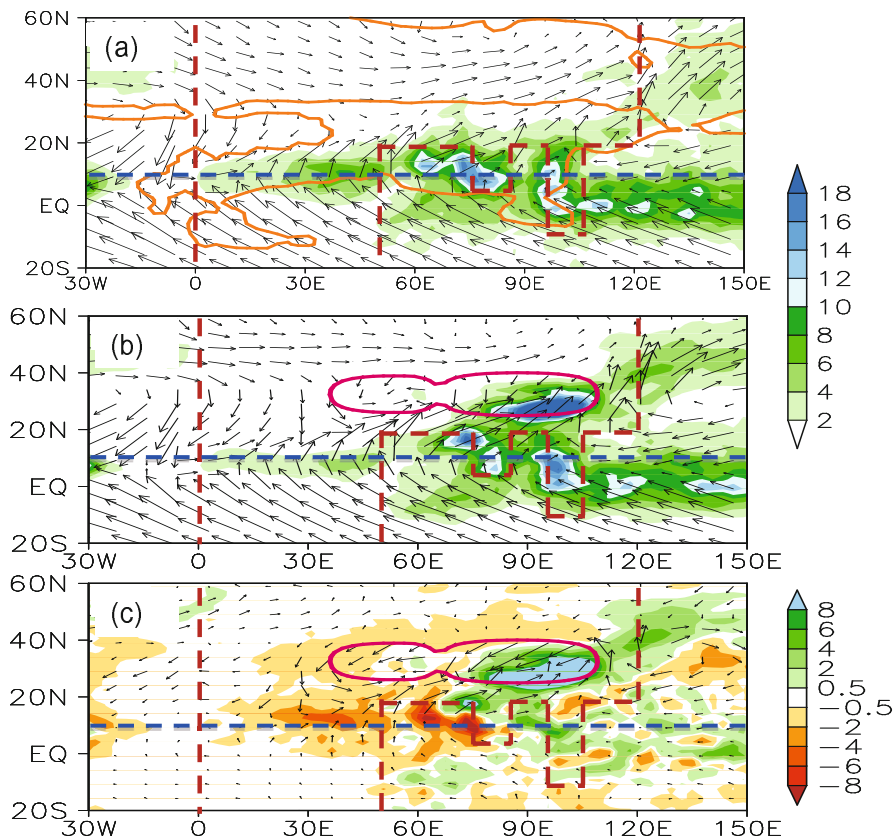
Fig. 11. July-mean wind vectors at $\sigma = 0.991$ (arrows; units: m s^{-1}) and precipitation (shading; units: mm d^{-1}) in experiment (a) TRO, (b) TPIR, and (c) their difference (TPIR − TRO). The heavy curve denotes the orographic contour at 700 m, the heavy red dashed line denotes the continental boundary, and the heavy blue dashed line indicates the 10°N, where the southern branch of the SASM is located. Refer to Fig. 10 in Wu et al. (2009, 2012a) and Fig. 6 in Liang et al. (2005).

subtropical M-AMC circulation? According to the criteria for defining the thermal equilibrium regime and AMC regime proved by Plumb and Hou (1992), small and even negative absolute vorticity occurring in the subtropics is conducive to the development of the AMC regime. To understand how the subtropical M-AMC is generated, Wu et al. (2016b) conducted another series of summertime AGCM experiments, one of which was a control experiment and the other was the same except the surface sensible heating over the main TP with elevation higher than 2 km was not allowed to heat the atmosphere. By calculating the difference between the results, the impacts of the surface sensible heating over the main TP could be evaluated. Figure 13a shows the difference between the results of the two experiments in terms of the distribution of absolute vorticity at the 150-hPa level. The TP heating produces a belt of negative absolute vorticity difference between 30°N and 40°N. A remarkable negative absolute vorticity difference center of more than -1.5×10^{-5} s^{-1} is located over the Pamir. Accordingly, along 35°N, a negative potential vorticity (PV) difference develops over the TP, with a strong negative center of more than −1 PVU lo-

cated over the western TP and near the tropopause (Fig. 13b). These results demonstrate that the TP surface sensible heating causes significant changes in the upper-tropospheric temperature and circulation above the TP, resulting in minimum static stability (not shown), absolute vorticity, and PV near the tropopause. According to the criteria of Plumb and Hou (1992), the subtropical M-AMC meridional circulation is generated. The north–south horizontal advection of absolute vorticity in such an M-AMC meridional circulation is negative in the lower troposphere and positive in the upper troposphere. According to Eq. (1), a background of large-scale ascending air in the ASM area is thus produced due to the TP thermal forcing.

The results reviewed in this section demonstrate that, in addition to its pumping effects on the atmospheric circulation, the AHS over the TP—particularly its surface sensible heating—can produce minimum absolute vorticity and PV above the TP through changing the atmospheric thermal structure. Subject to the AMC constraint, a strong subtropical monsoonal-type meridional circulation is thus generated, and large-scale ascending air is produced over the vast ASM area,
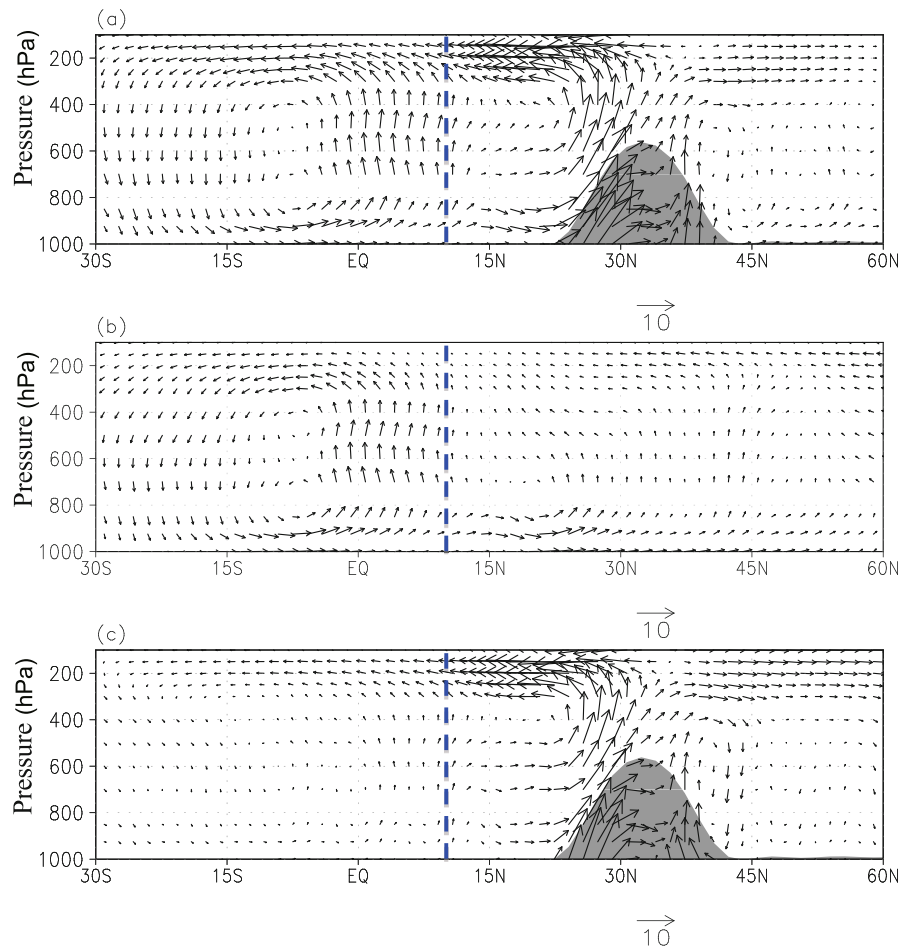
Fig. 12. Mean meridional circulation $(v, -\omega)$ averaged over the eastern continental domain between 90°E and 120°E in experiment (a) TPO, (b) TPIR, and (c) their difference (TRIP − TRO). The vertical coordinate is in hPa. The shading in (b, c) denotes the TP's shape across 87.5°E. The vertical pressure velocity ω is amplified by 60 in the plots. The heavy blue dashed line indicates the 10°N, where the southern branch of the SASM is located. [Reprinted from Wu et al. (2012a)].

which provides a favorable background for the development of the ASM.

5. Concluding remarks

This review comprises three parts: an assessment of the uncertainty and applicability of various data resources concerning the AHS over the TP; the formation of the AHS over the TP and its interaction with the atmospheric circulation; and the roles of TP forcing in the formation of the M-AMC type meridional circulation and the ASM.

It has been demonstrated that considerable uncertainty exists in the spatial pattern of the AHS over the TP, differing from one dataset to another. Such uncertainty is present in reanalysis data because the modeled climate usually deviates from the observed climate. However, the mean AHS averaged over the TP is applicable in studies on variation because, in

such circumstances, the bias of the modeled mean climate can to a large extent be eliminated. The review of results from analyses of the formation of the TP AHS reveals that the TP AHS is not only the cause of the atmospheric circulation, but also a result of that circulation. From numerical experiments, the land–sea thermal contrast only accounts for one part of the tropical monsoon. The surface sensible heating of the Iranian Plateau and TP plays a significant role in the formation of the ASM; in addition to its effects in pumping water vapor from sea to land and from the lower to upper troposphere to feed the continental monsoonal precipitation, it also generates a strong subtropical monsoonal meridional circulation subject to the AMC constraint, which provides the ascending-motion background necessary for the development and maintenance of the ASM. From these aspects, we can conclude that the Asian monsoon is formed because of the response of the atmospheric circulation to the seasonal changes in land–sea thermal contrast and the thermal
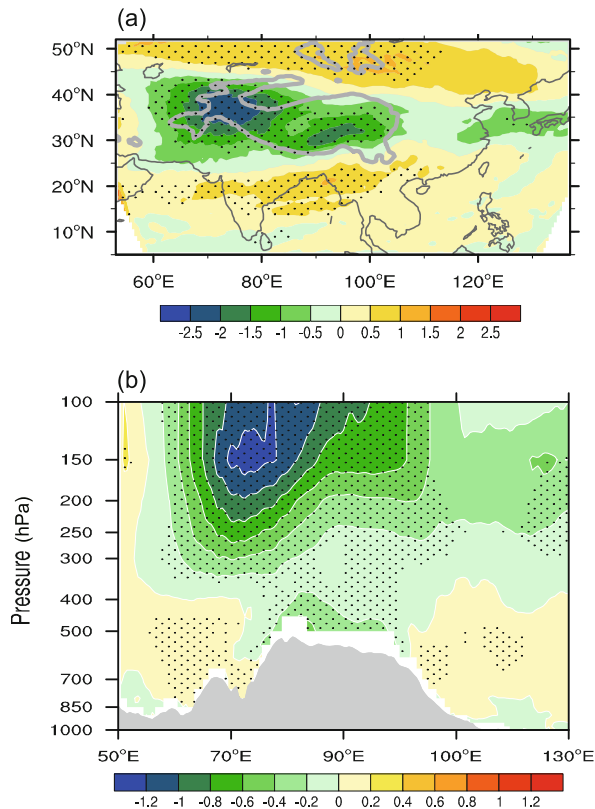
Fig. 13. Distribution of the difference between the experiments with and without surface sensible heating over the main body of the TP: (a) absolute vorticity at 150 hPa (shading; units: 10^{-5} s^{-1}). The gray contour denotes TP topography; (b) PV along 35°N (units: PVU = 10^{-6} K m^2 s^{-1} kg^{-1}). The gray shading denotes topography. Dotted regions denote that the statistical significance of the difference is above the 95% level. [Reprinted from Wu et al. (2016b)].

status of the large-scale orography. However, this does not mean that the mechanical forcing of the TP is not important to the ASM. Actually, when the southwesterly flow in the lower troposphere impinges on the Hengduan Mountains, it cannot climb over but is instead deflected and turns to easterly flow along the slope of the TP, forming the monsoon trough over North India. Although the TP exerts direct impacts on the Asian monsoon and climate, the thermal conditions over the TP are influenced by the forcing from the atmosphere, the cryosphere, and the remote oceans. Further studies, therefore, are required to understand how the AHS over the TP is formed, and how the TP, together with other mechanisms, affects weather and climate.

REFERENCES

Alessandri, C., and N. VenturiGinori, 1931: Meteorologia, Aerologia e Pireliometria. *Spedizione Italiana de Filippi*, Serie I, Bologna, 3.(In Italian)

Chen, L. X., and W. Li, 1981: The summer atmospheric heat budget in the Asian monsoon area. *Collection of the National Conference on the Tropical Summer Monsoon*, Vol. I., Yunnan People's Press, 86–101. (in Chinese)

Chen, L. X., and W. Li, 1982: Structure of the monthly mean atmospheric heat source in the Asian monsoon area. *Collection of the National Conference on the Tropical Summer Monsoon*, Vol. II., Yunnan People's Press, 246–258. (in Chinese)

Chen, L. X., E. R. Reiter, and Z. Q. Feng, 1985: The atmospheric heat source over the Tibetan Plateau: May August 1979. *Mon. Wea. Rev.*, **113**(10), 1771–1790, doi: 10.1175/1520-0493(1985)113<1771:TAHSOT>2.0.CO;2.

Chen, L. X., F. Schmidt, and W. Li, 2003: Characteristics of the atmospheric heat source and moisture sink over the Qinghai-Tibetan Plateau during the Second TIPEX of summer 1998 and their impact on surrounding monsoon. *Meteor. Atmos. Phys.*, **83**(1–2), 1–18, doi: 10.1007/s00703-002-0546-x.

Chu, P. C., 1957a: The steady state perturbations of the westerlies by the large-scale heat sources, sinks and earth's orography (I)—The distribution of heat sources and sinks in lower troposphere over northern hemisphere. *Acta Meteorologica Sinica*, **28**, 122–140, doi: 10.11676/qxxb1957.011. (in Chinese with English abstract)

Chu, P. C., 1957b: The steady state perturbations of the westerlies by the large-scale heat sources and sinks and earth's orography (II). *Acta Meteorologica Sinica*, **28**, 198–224. (in Chinese with English abstract)

Chu, P. C., 1957c: Role of large-scale mountain in the formation of temperature field. *Acta Meteorologica Sinica*, **28**, 315–318. (in Chinese)

Duan, A. M., and G. X. Wu, 2008: Weakening trend in the atmospheric heat source over the Tibetan Plateau during recent decades. Part I: Observations. *J. Climate*, **21**(13), 3149–3164, doi: 10.1175/2007JCLI1912.1.

Duan, A. M., and G. X. Wu, 2009: Weakening trend in the atmospheric heat source over the Tibetan Plateau during recent decades. Part II: Connection with climate warming. *J. Climate*, **22**, 4197–4212, doi: 10.1175/2009JCLI2699.1.

Duan, A. M., M. R. Wang, and Z. X. Xiao, 2014: Uncertainties in quantitatively estimating the atmospheric heat source over the Tibetan Plateau. *Atmospheric and Oceanic Science Letters*, **7**, 28–33, doi: 10.1080/16742834.2014.11447131.

Flohn, H., 1957: Large-Scale aspects of the "summer monsoon" in South and East Asia. *J. Meteor. Soc. Japan*, **75**, 180–186, doi: 10.2151/jmsj1923.35A.0_180.

He, J. H., H. M. Xu, S. S. Zhong, Y. F. Gong, L. P. Li, and B. Zhang, 2011: *Characteristics of the Atmospheric Heating Source Over the Tibetan Plateau, Its Impacts and Potential Mechanism*. Beijing, China Meteor. Press, 243 pp. (in Chinese)

Held, I. M., 1983: Stationary and quasi-stationary eddies in the extratropical troposphere: Theory. *Large-Scale Dynamical Principles in the Atmosphere*, B. Hoskins and R. Pearce, Eds.,

Academic Press, 127–168.

Held, I. M., and A. Y. Hou, 1980: Nonlinear axially symmetric circulations in a nearly inviscid atmosphere. *J. Atmos. Sci.*, **37**(3), 515–533, doi: 10.1175/1520-0469(1980)037<0515: NASCIA>2.0.CO;2.

Jiang, X. W., Y. Q. Li, S. Yang, K. Yang, and J. W. Chen, 2016: Interannual variation of summer atmospheric heat source over the Tibetan plateau and the role of convection around the western maritime continent. *J. Climate*, **29**, 121–138, doi: 10.1175/JCLI-D-15-0181.1.

Kuo, H. L., and Y. F. Qian, 1982: Numerical simulation of the development of mean monsoon circulation in July. *Mon. Wea. Rev.*, **110**, 1879–1897, doi: 10.1175/1520-0493(1982)110 <1879:NSOTDO>2.0.CO;2.

Li, C. F., and M. Yanai, 1996: The onset and interannual variability of the Asian summer monsoon in relation to land–sea thermal contrast. *J. Climate*, **9**, 358–375, doi: 10.1175/1520-0442(1996)009<0358:TOAIVO>2.0.CO;2.

Liang, X. Y., Y. M. Liu, and G. X. Wu, 2005: The role of land-sea distribution in the formation of the Asian summer monsoon. *Geophys. Res. Lett.*, **32**, L03708, doi: 10.1029/2004GL 021587.

Liu, Y. M., B. Hoskins, and M. Blackburn, 2007: Impact of Tibetan orography and heating on the summer flow over Asia (125th anniversary issue of the meteorological society of Japan). *J. Meteor. Soc. Japan*, **85B**, 1–19.

Liu, Y. M., G. X. Wu, J. L. Hong, B. W. Dong, A. M. Duan, Q. Bao, and L. J. Zhou, 2012: Revisiting Asian monsoon formation and change associated with Tibetan Plateau forcing: II. Change. *Climate Dyn.*, **39**(5), 1183–1195, doi: 10.1007/ s00382-012-1335-y.

Luo, H. B., and M. Yanai, 1984: The large-scale circulation and heat sources over the Tibetan Plateau and surrounding areas during the early summer of 1979. Part II: Heat and moisture budgets. *Mon. Wea. Rev.*, **112**, 966–989, doi: 10.1175/1520-0493(1984)112<0966:TLSCAH>2.0.CO;2.

Ma, Y., and Coauthors, 2014a: Combining MODIS, AVHRR and in situ data for evapotranspiration estimation over heterogeneous landscape of the Tibetan Plateau. *Atmospheric Chemistry and Physics*, **14**, 1507–1515, doi: 10.5194/acp-14-1507-2014.

Ma, Y. M., and Coauthors, 2014b: Using MODIS and AVHRR data to determine regional surface heating field and heat flux distributions over the heterogeneous landscape of the Tibetan Plateau. *Theor. Appl. Climatol.*, **117**(3-4), 643–652, doi: 10.1007/s00704-013-1035-5.

Molnar, P., and K. A. Emanuel, 1999: Temperature profiles in radiative-convective equilibrium above surfaces at different heights. *J. Geophys. Res.*, **104(D20)**, 24265–24271, doi: 10.1029/1999JD900485.

Pan, W. J., J. Y. Mao, and G. X. Wu, 2013: Characteristics and mechanism of the 10-20-day oscillation of spring rainfall over southern China. *J. Climate*, **26**, 5072–5087, doi: 10.1175/ JCLI-D-12-00618.1.

Plumb, R. A., and A. Y. Hou, 1992: The response of a zonally symmetric atmosphere to subtropical thermal forcing: Threshold behavior. *J. Atmos. Sci.*, **49**, 1790–1799, doi: 10.1175/1520-0469(1992)049<1790:TROAZS>2.0.CO;2.

Schneider, E. K., 1977: Axially symmetric steady-state models of the basic state for instability and climate studies. Part II. Nonlinear calculations. *J. Atmos. Sci.*, **34**(2): 280–296, doi: 10.1175/1520-0469(1977)034<0280:ASSSMO>2.0.CO;2.

Schneider, E. K., 1987: A simplified model of the modified Hadley circulation. *J. Atmos. Sci.*, **44**(22), 3311–3328, doi: 10.1175/ 1520-0469(1987)044<3311:ASMOTM>2.0.CO;2.

Schneider, E. K., and R. S. Lindzen, 1977: Axially symmetric steady-state models of the basic state for instability and climate studies. Part I. Linearized calculations. *J. Atmos. Sci.*, **34**(2): 263–279, doi: 10.1175/1520-0469(1977)034<0263: ASSSMO>2.0.CO;2.

Seto, R., T. Koike, and M. Rasmy, 2013: Analysis of the vertical structure of the atmospheric heating process and its seasonal variation over the Tibetan Plateau using a land data assimilation system. *J. Geophys. Res.*, **118**, 12 403–12 421, doi: 10.1002/2013JD020072.

Tamura, T., K. Taniguchi, and T. Koike, 2010: Mechanism of upper tropospheric warming around the Tibetan Plateau at the onset phase of the Asian summer monsoon. *J. Geophys. Res.*, **115**(D2), D02106, doi: 10.1029/2008JD011678.

Taniguchi, K., and T. Koike, 2007: Increasing atmospheric temperature in the upper troposphere and cumulus convection over the eastern part of the Tibetan Plateau in the pre-monsoon season of 2004. *J. Meteor. Soc. Japan.*, **85A**, 271–294, doi: 10.2151/jmsj.85A.271.

Taniguchi, K., T. Tamura, T. Koike, K. Ueno, and X. D. Xu, 2012: Atmospheric conditions and increasing temperature over the Tibetan Plateau during early spring and the pre-monsoon season in 2008. *J. Meteor. Soc. Japan.*, **90C**, 17–32, doi: 10.2151/jmsj.2012-C02.

Tian, S. F., and T. Yasunari, 1998: Climatological aspects and mechanism of spring persistent rains over central China. *J. Meteor. Soc. Japan.*, **76**(1), 57–71.

Wan, R. J., and G. X. Wu, 2007: Mechanism of the Spring Persistent Rains over southeastern China. *Sciences in China D: Earth Sciences*, **50**, 130–144.

Webster, P. J., V. O. Magaña, T. N. Palmer, J. Shukla, R. A. Tomas, M. Yanai, and T. Yasunari, 1998: Monsoons: Processes, predictability, and the prospects for prediction. *J. Geophys. Res.*, **103**, 14 451–14 510, doi: 10.1029/97JC02719.

Wu, G. X., and Y. S. Zhang, 1998: Tibetan plateau forcing and the timing of the monsoon onset over South Asia and the South China Sea. *Mon. Wea. Rev.*, **126**, 913–927, doi: 10.1175/ 1520-0493(1998)126<0913:TPFATT>2.0.CO;2.

Wu, G. X., H. F. Zhuo, Z. Q. Wang, and Y. M. Liu, 2016b: Two types of summertime heating over the Asian large-scale orography and excitation of potential-vorticity forcing I. Over Tibetan Plateau. *Science China Earth Sciences*, **59**(10), 1996–2008, doi: 10.1007/s11430-016-5328-2.

Wu, G. X., B. He, Y. M. Liu, Q. Bao, and R. C. Ren, 2015b: Location and variation of the summertime upper-troposphere temperature maximum over South Asia. *Climate Dyn.*, **45**, 2757–2774, doi: 10.1007/s00382-015-2506-4.

Wu, G. X., W. P. Li, H. Guo, H. Liu, J. S. Xue, and Z. Z. Wang, 1997: Sensible heat driven air-pump over the Tibetan Plateau and its impacts on the Asian Summer Monsoon. *Collections on the Memory of Zhao Jiuzhang*, Y. Duzheng, Ed., Science Press, 116–126. (in Chinese)

Wu, G. X., Y. M. Liu, B. He, Q. Bao, A. M. Duan, and F. F. Jin, 2012b: Thermal controls on the Asian summer monsoon. *Scientific Reports*, **2**, 404, doi: 10.1038/srep00404.

Wu, G. X., B. Hu, Y. M. Liu, Q. Bao, R. C. Ren, and B. Q. Liu, 2016a: Recent progresses on dynamics of the Tibetan Plateau and Asian summer monsoon. *Chinese Journal of Atmospheric Sciences*, **40**(1), 22–32, doi: 10.3878/j.issn.1006-

9895.1504.15129. (in Chinese with English abstract)

Wu, G. X., Y. M. Liu, X. Zhu, W. Li, R. C. Ren, A. M. Duan, and X. Liang, 2009: Multi-scale forcing and the formation of subtropical desert and monsoon. *Annales Geophysicae*, **27**, 3631–3644, doi: 10.5194/angeo-27-3631-2009.

Wu, G. X., Y. M. Liu, B. W. Dong, X. Y. Liang, A. M. Duan, Q. Bao, and J. J. Yu, 2012a: Revisiting Asian monsoon formation and change associated with Tibetan Plateau forcing: I. Formation. *Climate Dyn.*, **39**(5), 1169–1181, doi: 10.1007/s00382-012-1334-z.

Wu, G. X., and Coauthors, 2007: The influence of mechanical and thermal forcing by the Tibetan Plateau on Asian climate. *Journal of Hydrometeorology*, **8**(4), 770–789, doi: 10.1175/JHM609.1.

Wu, G. X., and Coauthors, 2015a: Tibetan Plateau climate dynamics: Recent research progress and outlook. *National Science Review*, **2**(1), 100–116, doi: 10.1093/nsr/nwu045.

Yanai, M., C. F. Li, and Z. S. Song, 1992: Seasonal heating of the Tibetan Plateau and its effects on the evolution of the Asian summer monsoon. *J. Meteor. Soc. Japan*, **70**, 319–351, doi: 10.2151/jmsj1965.70.1B_319.

Yang, J. C., and S. W. Lo, 1957: Study of the circulation and heating feature over the Tibetan Plateau based on surface observation. *Acta Meteorologica Sinica*, **28**, 264–274, doi: 10.11676/qxxb1957.022. (in Chinese)

Yang, K., Y. Y. Chen, and J. Qin, 2009: Some practical notes on the land surface modeling in the Tibetan Plateau. *Hydrology and Earth System Sciences*, **13**, 687–701, doi: 10.5194/hess-13-687-2009.

Yang, K., X. F. Guo, and B. Y. Wu, 2011b: Recent trends in surface sensible heat flux on the Tibetan Plateau. *Science China Earth Sciences*, **54**, 19–28, doi: 10.1007/s11430-010-4036-6.

Yang, K., X. F. Guo, J. He, J. Qin, and T. Koike, 2011a: On the climatology and trend of the atmospheric heat source over the Tibetan Plateau: An experiments-supported revisit. *J. Climate*, **24**, 1525–1541, doi: 10.1175/2010JCLI3848.1.

Yeh, T. C., S. W. Lo, and P. C. Chu, 1957: The wind structure and heat balance in the lower troposphere over Tibetan plateau and its surrounding. *Acta Meteorologica Sinica*, **28**, 108–121, doi: 10.11676/qxxb1957.010. (in Chinese with English abstract)

Yu, J. J., Y. M. Liu, and G. X. Wu, 2011a: An analysis of the diabatic heating characteristic of atmosphere over the Tibetan Plateau in winter I: Climatology. *Acta Meteorologica Sinica*, **69**(1), 79–88, doi: 10.11676/qxxb2011.007. (in Chinese with English abstract)

Yu, J. J., Y. M. Liu, and G. X. Wu, 2011b: An analysis of the diabatic heating characteristic of atmosphere over the Tibetan Plateau in winter II: Interannual variation. *Acta Meteorologica Sinica*, **69**(1), 89–98, doi: 10.11676/qxxb2011.008. (in Chinese with English abstract)

Zhang, J. J., G. W. Sun, and B. D. Chen, 1991: *Research on Atmospheric Low-Frequency Variations over the Qinghai-Xizang Plateau*. Meteorological Press, 1–109. (in Chinese)

Zhao, P., and L. X. Chen, 2001: Interannual variability of atmospheric heat source/sink over the Qinghai–Xizang (Tibetan) Plateau and its relation to circulation. *Adv. Atmos. Sci.*, **18**, 106–116, doi: 10.1007/s00376-001-0007-3.

Zhou, T. J., D. Y. Gong, J. Li, and B. Li, 2009: Detecting and understanding the multi-decadal variability of the East Asian summer monsoon recent progress and state of affairs. *Meteorologische Zeitschrift*, **18**(4), 455–467, doi: 10.1127/0941-2948/2009/0396.

Zhu, X. Y., Y. M. Liu, and G. X. Wu, 2012: An assessment of summer sensible heat flux on the Tibetan Plateau from eight data sets. *Science China Earth Sciences*, **55**(5), 779–786, doi: 10.1007/s11430-012-4379-2.